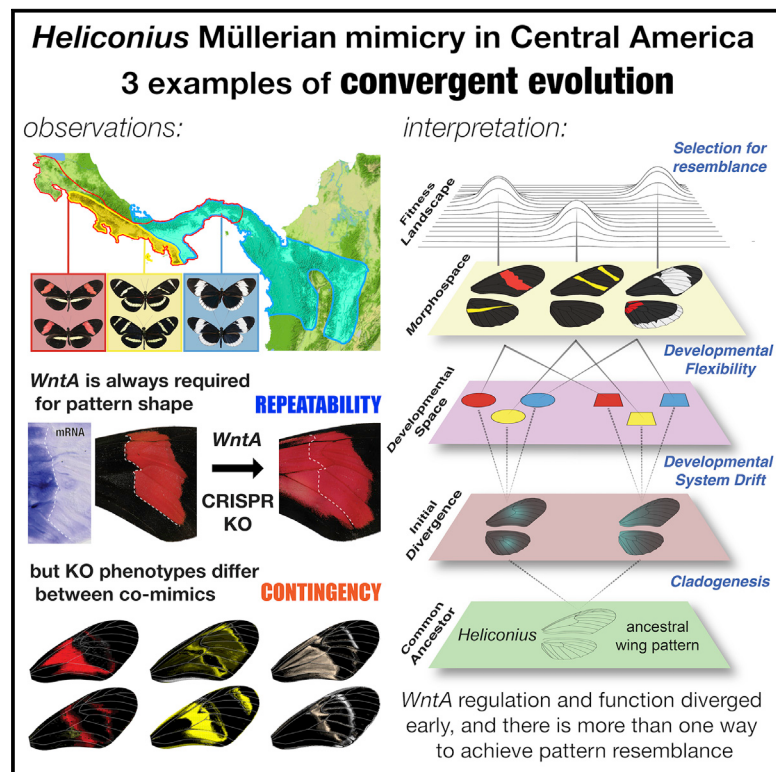


Interplay between Developmental Flexibility and Determinism in the Evolution of Mimetic *Heliconius* Wing Patterns

Graphical Abstract



Authors

Carolina Concha,
Richard W.R. Wallbank,
Joseph J. Hanly, ..., Riccardo Papa,
Arnaud Martin, W. Owen McMillan

Correspondence

carolacmcl@yahoo.com

In Brief

Concha et al. use CRISPR/Cas9 genome editing to knock out a major wing patterning gene, *WntA*, in mimetic species of *Heliconius* butterflies and report that *WntA* is used in divergent gene regulatory networks in co-mimics and that resemblance is achieved through differential expression of *WntA* and its interaction with the specific genetic background.

Highlights

- Mimicry in *Heliconius* is achieved through divergent developmental networks
- WntA* is a major patterning gene that is used differently in co-mimics
- Regulation of *WntA* expression and its interaction with other genes shape diversity
- WntA* modulates wing-scale cell identity



Interplay between Developmental Flexibility and Determinism in the Evolution of Mimetic *Heliconius* Wing Patterns

Carolina Concha,^{1,11,13,*} Richard W.R. Wallbank,^{1,2} Joseph J. Hanly,^{1,3} Jennifer Fenner,⁴ Luca Livraghi,^{1,5} Edgardo Santiago Rivera,^{1,6} Daniel F. Paulo,^{1,7} Carlos Arias,¹ Marta Vargas,¹ Manu Sanjeev,¹ Colin Morrison,¹ David Tian,¹ Paola Aguirre,¹ Sabrina Ferrara,¹ Jessica Foley,¹ Carolina Pardo-Diaz,⁸ Camilo Salazar,⁸ Mauricio Linares,⁸ Darli Massardo,⁹ Brian A. Counterman,⁴ Maxwell J. Scott,¹⁰ Chris D. Jiggins,^{1,5} Riccardo Papa,^{1,6,11,12} Arnaud Martin,^{3,12} and W. Owen McMillan^{1,12}

¹Smithsonian Tropical Research Institute, Apartado 0843-03092, Panama City, Panama

²Dunn School of Pathology, University of Oxford, Oxford OX1 3RE, UK

³Department of Biological Sciences, The George Washington University, Washington, DC 20052, USA

⁴Department of Biological Sciences, Mississippi State University, 295 Lee Boulevard, Mississippi State, MS 39762, USA

⁵Department of Zoology, University of Cambridge, Cambridge CB2 3EJ, UK

⁶Department of Biology, Center for Applied Tropical Ecology and Conservation, University of Puerto Rico, Rio Piedras Campus, San Juan 00931, Puerto Rico

⁷Departamento de Genética, Evolução e Bioagentes, Instituto de Biologia, Universidade Estadual de Campinas, Campinas, SP 13083-875, Brazil

⁸Biology Program, Faculty of Natural Sciences and Mathematics, Universidad del Rosario, Carrera. 24 No. 63C-69, Bogota, DC 111221, Colombia

⁹Department of Ecology and Evolution, University of Chicago, Chicago, IL 60637, USA

¹⁰Department of Entomology and Plant Pathology, North Carolina State University, Campus Box 7613, Raleigh, NC 27695-7613, USA

¹¹Molecular Sciences and Research Center, University of Puerto Rico, San Juan 00907, Puerto Rico

¹²These authors contributed equally

¹³Lead Contact

*Correspondence: carolacmcl@yahoo.com

<https://doi.org/10.1016/j.cub.2019.10.010>

SUMMARY

To what extent can we predict how evolution occurs? Do genetic architectures and developmental processes canalize the evolution of similar outcomes in a predictable manner? Or do historical contingencies impose alternative pathways to answer the same challenge? Examples of Müllerian mimicry between distantly related butterfly species provide natural replicates of evolution, allowing us to test whether identical wing patterns followed parallel or novel trajectories. Here, we explore the role that the signaling ligand *WntA* plays in generating mimetic wing patterns in *Heliconius* butterflies, a group with extraordinary mimicry-related wing pattern diversity. The radiation is relatively young, and numerous cases of wing pattern mimicry have evolved within the last 2.5–4.5 Ma. *WntA* is an important target of natural selection and is one of four major effect loci that underlie much of the pattern variation in the group. We used CRISPR/Cas9 targeted mutagenesis to generate *WntA*-deficient wings in 12 species and a further 10 intraspecific variants, including three co-mimetic pairs. In all tested butterflies, *WntA* knockouts affect pattern broadly and cause a shift among every possible scale cell type. Interestingly, the co-

mimics lacking *WntA* were very different, suggesting that the gene networks that pattern a wing have diverged considerably among different lineages. Thus, although natural selection channeled phenotypic convergence, divergent developmental contexts between the two major *Heliconius* lineages opened different developmental routes to evolve resemblance. Consequently, even under very deterministic evolutionary scenarios, our results underscore a surprising unpredictability in the developmental paths underlying convergence in a recent radiation.

INTRODUCTION

Evolution is often viewed as a highly contingent process, where chance mutations and random genetic drift affect future outcomes. Nonetheless, there are many cases across branches of the tree of life where different species have evolved remarkably similar solutions to common environmental challenges. Such convergence provides some of the most compelling evidence of the power of natural selection to shape phenotypic diversity in highly deterministic ways. Over the past several decades, numerous studies have examined how convergent change is achieved (reviewed recently in [1]). The broad consensus emerging from these studies is that the path taken by evolution is often repeatable among closely related species but becomes more unpredictable when species are deeply divergent [1, 2].



Most of these studies center on whether convergent phenotypes are achieved using similar morphological and/or genetic changes (see [3] for an excellent recent example). Although highly illuminating, these studies largely ignore changes in the developmental pathways that are ultimately responsible for many phenotypic traits. The relationship between genotype and phenotype is complicated, and there is a growing appreciation that gene regulatory networks (GRNs) can diverge rapidly [4]. This divergence creates a complex set of historical contingencies that we are only beginning to appreciate (see [5–7]).

Here, we use the patterns on butterfly wings to explore the interplay between developmental change and determinism in the evolution of convergent phenotypes. Across the Lepidoptera, natural and sexual selection have acted on developmental processes to create a staggering array of wing patterns. Underlying this diversity is the evolution of specialized scale cells that cover the wing surface, combined with a spatial coordinate system that controls their pigment production and ultrastructural complexity [8]. As a morphological trait, wing patterns are two dimensional, with color and pattern mapping directly onto a developing wing. As such, they represent an excellent system in which the transitions from genes, through developmental pathways, to phenotype and fitness can be clearly illuminated.

Butterfly wing pattern diversity includes numerous instances of mimicry where distantly related species converge on nearly identical wing patterns. Indeed, cases of wing pattern mimicry among a toxic and non-toxic species (Batesian mimicry) [9] and among toxic species (Müllerian mimicry) [10] abound. One unresolved question is the extent to which similar or distinct mechanisms have generated convergent phenotypes [11]; in other words, are phenotypic repeats based on parallel reiterations of the same process or do distinct developmental roads lead to the same destination? Butterfly wing patterns share a history dating back about 120 Ma [12], which might predispose them to evolve in similar ways, particularly among more closely related lineages. However, a number of recent studies have demonstrated extraordinary flexibility in the way in which patterning networks are deployed to generate variation. For example, the eyespot patterns that are found in many nymphalid butterflies appear to have evolved once; but the gene regulatory networks underlying these patterns have diverged significantly over the past 65 Ma such that the eyespots of different species are controlled by different sets of genes [13].

In this study, we explore the basis of convergent wing pattern change within *Heliconius*, a group of neotropical butterflies renowned for wing pattern variation. The extraordinary diversity in wing patterns among the 48 species in the genus arose within the last 12–14 Ma [14] and includes remarkable pattern convergence between distantly related species, as well as marked pattern divergence between closely related populations and species. Patterns serve to warn potential predators of the butterflies' unpalatability and provide one of nature's most notable examples of Müllerian mimicry [15–17]. Recent work has identified four major effect loci, *optix*, *aristaless 1*, *WntA*, and *cortex*, that are direct targets of natural selection and modulate much of the pattern diversity across the genus [18–21].

Within *Heliconius*, we focus on two lineages, the *H. erato*/*sapho*/*sara* (ESS) and the *H. melpomene*/*cyclone*/*silvaniform* (MCS) species groups (Figure 1A), to explore how phenotypic

convergence is achieved. The two lineages diverged from a common ancestor early in the formation of the genus and have been evolving separately for the past 12 Ma, diverging in many aspects of their ecology and reproductive biology [22–24]. Nonetheless, within the last 2.5–4.5 Ma, the groups have converged on a similar complement of wing pattern types, including a number of cases of near-perfect wing pattern mimicry. In Panama, for example, the species pairs *H. erato demophoon* (ESS)/*H. melpomene rosina* (MCS), *H. sapho sapho* (ESS)/*H. cycloneus* (MCS), and *H. hewitsoni* (ESS)/*H. pachinus* (MCS) are near perfect mimics of each other (Figure 1B), providing replicated cases of convergent adaptive evolution. Although hybridization and introgression play a role in the evolution of novel patterns within the ESS and MCS clades [25, 26], there is no evidence for hybridization between the two groups. As a result, there is a substantial history where drift, mutation, and selection caused the accumulation of genetic differences between the two lineages. From these different starting points, we are specifically interested in the functional role that the gene *WntA* plays in generating pattern variation.

WntA is a widespread member of the Wnt family of signaling ligands that has been lost in vertebrates and *Drosophila*, with RNAi evidence in *Tribolium* beetles suggesting it is not required for insect embryogenesis in spite of its segmental expression [27]. Perhaps because it is less constrained than its paralogs, *WntA* has evolved new roles and notably fueled forewing pattern shape variation in *Heliconius* [28–35], with repeated *cis*-regulatory modification of this gene underlying phenotypic divergence [36, 37]. The result is drastic shifts in *WntA* expression between close relatives despite almost no coding variation in the *WntA* protein across the entire genus. Interestingly, variation in regulatory regions of this locus is also responsible for mimicry-related pattern differences between mimetic and non-mimetic morphs of *Limenitis arthemis* [34]. Based on this evolutionary conservation, we hypothesize that robust phenotypic convergence occurs in this system via one of two alternative scenarios. First, under a deterministic scenario, *WntA* may be ancestrally predisposed to yield certain morphologies. If this is true, we expect that *WntA* is responsible for very similar phenotypic effects in co-mimics. Thus, *WntA* knockout (KO) phenotypes should be similar or identical. Alternatively, the gene networks responsible for patterning a wing might have diverged in the two lineages, such that new regulatory connections around *WntA*, the loci that respond to *WntA* signals, and other patterning loci have changed. If this is the case, we would predict different functional effects of *WntA* on pattern between co-mimics.

We test these alternatives by functionally knocking out *WntA* in three co-mimic pairs using CRISPR-Cas9 genome editing [38, 39]. Moreover, we cast our results broadly by knocking out *WntA* across an additional 6 *Heliconius* species, including *H. doris* from a third divergent lineage and nearly a dozen different intraspecific wing color pattern morphs of *H. erato*. These experiments underscore a diverse regulatory architecture around *WntA*, highlighting differences in how *WntA* signals are interpreted, and reveal hidden variation in other wing patterning loci. Divergence in all these factors accumulates quickly among lineages and provides an array of different paths for natural selection to shape pattern variation.

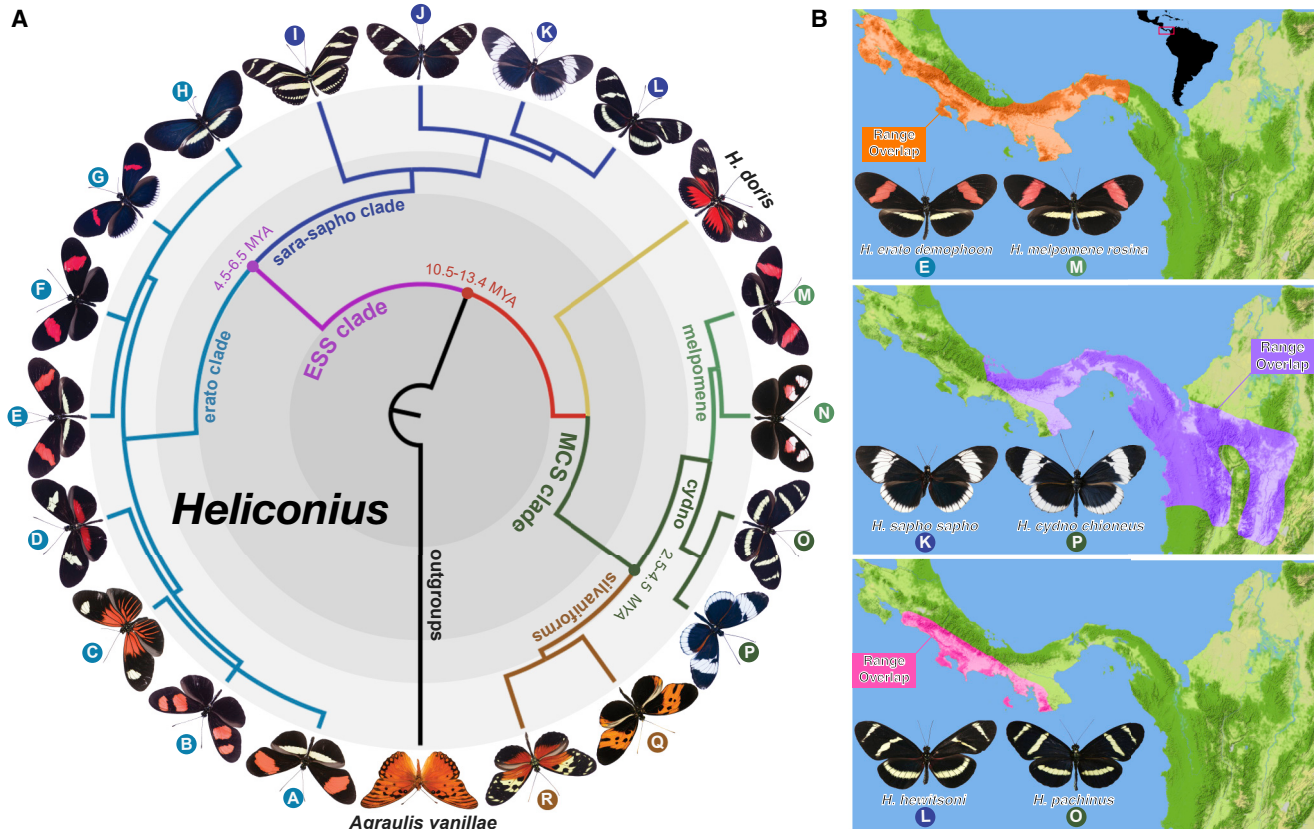


Figure 1. The *Heliconius* Color Pattern Radiation

(A) Wing pattern variation across a phylogeny of species and morphs used in the present study with *Agraulis vanillae* defined as the outgroup. The *erato/sara* (*ESS*) group species includes *H. e. favorinus* (A), *H. e. microclea* (B), *H. e. etylus* (C), *H. himera* (D), *H. e. demophoon* (E), *H. e. hydara* (F), *H. e. cyrbia* (G), *H. e. chestertonii* (H), *H. charitonia* (I), *H. sara* (J), *H. sapho* (K), and *H. hewitsoni* (L). The *melpomene*, *cydno*, *silvaniform* (*MCS*) group species includes *H. m. amaryllis* (M), *H. m. plesseni* (N), *H. pachinus* (O), *H. cydno* (P), *H. numata* (Q), and *H. hecale* (R). *Heliconius doris* falls within a third lineage, roughly intermediate between the *ESS* and *MCS* groups. Approximate divergence times for the genus and for species within the *ESS* and *MCS* clade are derived from [14].

(B) Geographical distribution of the co-mimetic species studied. Top: *H. e. demophoon* (*ESS*)/*H. m. rosina* (*MCS*) is shown. Middle: *H. sapho sapho* (*ESS*)/*H. cydno chionoeus* (*MCS*) is shown. Bottom: *H. hewitsoni* (*ESS*)/*H. pachinus* (*MCS*) is shown.

RESULTS

Our *WntA* KO experiments sampled an extensive range of the phenotypic variation found in *Heliconius* and encompassed timescales ranging from 10 to 14 Ma (comparison between *ESS* and *MCS* lineages), 4.5 to 6.5 Ma (comparison within the *ESS* and *MCS* lineages), and 2.5 to 4.5 Ma (comparisons among *H. erato* color pattern morphs; Figure 1A). Across all species examined, egg and larval survival after injection was generally high, and 30% of eclosed G₀ adults showed a mutant phenotype (Table S1). Because only a percentage of the nuclei in the syncytial embryo are edited with CRISPR [39], we observed varying degrees of mosaicism in the mutant G₀ butterflies (see Figure S1 for range of mosaic phenotypes in *H. e. demophoon*). In order to preserve butterfly wings for photography and further study of their scales, mutant individuals were genotyped using leg tissue. *WntA* KO butterflies contained indels in 75%–82% of PCR products amplified from leg genomic DNA; whereas in butterflies injected with Cas9/gRNA complexes but lacking a mutant phenotype, only 5%–12% of the PCR products possessed indels across the targeted *WntA* exon (Figure S2; Table S2).

Mimicry Is Achieved through Different Developmental Networks

Our experimental design included three pairs of distantly related species that have evolved near-perfect wing pattern mimicry (Figure 1B), allowing us to test whether *WntA* functions similarly to create convergent phenotypes. In every case of wing pattern mimicry that we studied, the functional KO of *WntA* had very different phenotypes between co-mimetic pairs (Figure 2). Generally, *WntA* mosaic KOs resulted in color pattern shifts in areas of the forewing and hindwing that correspond to areas of wild-type (WT) *WntA* mRNA expression in the developing fifth instar larval wing disc. The most striking phenotypes were observed in the forewings, where the bulk of *WntA* regulatory alleles drive pattern shape variation in *Heliconius* [36, 37]. In *H. e. demophoon* (*ESS*), there was a strong relationship between larval *WntA* expression and the KO phenotype, both restricted to the proximal section of the forewing (Figures 2A and S1) [41]. In contrast, in the co-mimic *H. m. rosina* (*MCS*), *WntA* mRNA was located in a thin band that marked the proximal edge of the forewing red band, mirroring the subtler phenotypic effect of *WntA* KO in that part of the wing (Figures 2B and S3).

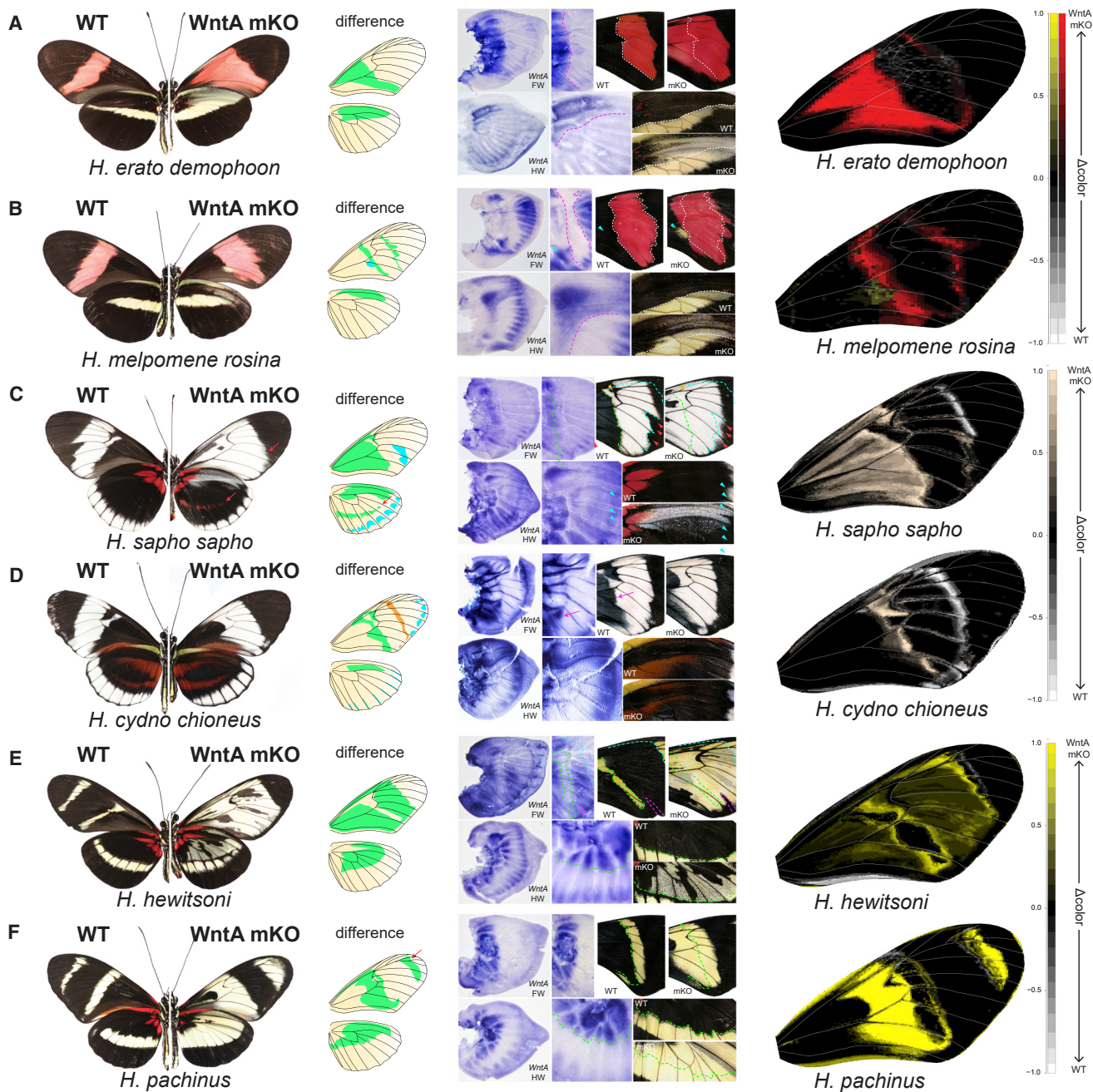


Figure 2. Mimicry in *Heliconius* Is Achieved by Different Developmental Mechanisms

WntA KO in the co-mimics *H. erato demophoon* (ESS; A), *H. melpomene rosina* (MCS; B), *H. sapho* (ESS; C), *H. cydno chioneus* (MCS; D), *H. hewitsoni* (ESS; E), and *H. pachinus* (MCS; F). The left and right side of each butterfly reflects the wild-type (WT) pattern and the mutant pattern (*WntA* KO), respectively. Further to the right (second panel) is a drawing highlighting the pattern difference between WT and KO patterns (green reflects loss of black patterns; yellow and blue reflect gain of black patterns in the middle and distal forewing, respectively), followed by *in situ* hybridizations showing the WT localization of *WntA* mRNA in developing wing discs, and a blow up of the midsection of the dorsal forewing and proximal section of the dorsal hindwing of the WT and *WntA* KO. Lines reflect the proximal and distal forewing band boundary and the proximal hindwing bar boundary. The final panel is a heatmap of the forewing showing the precise pattern differences between *WntA* mutants and WTs generated by overlaying five WT and five *WntA* KO wings using R/patternize [40]. See also Figures S1–S6 and Tables S1 and S2 for more detailed information.

WntA KO still affected the proximal boundary of the forewing band and caused an expansion of red proximally but over a much smaller portion of forewing surface. In addition, there was a switch from black to yellow in a small patch of scale cells

just below the proximal edge of the forewing band, something not observed in *H. e. demophoon*. In *H. melpomene*, *WntA* was also expressed distally, while the KO phenotype showed only a slight expansion of the distal red boundary (Figures 2B

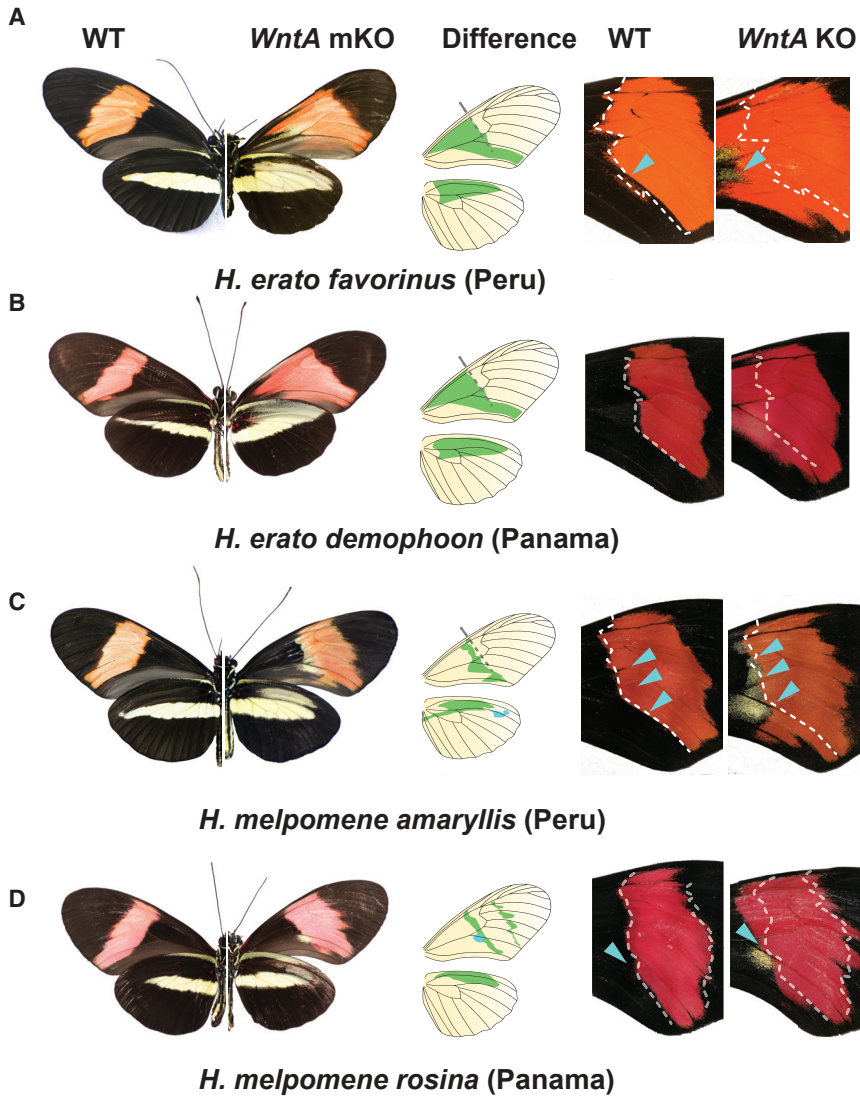


Figure 3. Co-mimetic *Heliconius* Pairs from Different Geographical Locations Show Slightly Diverse *WntA* Loss-of-Function Phenotypes

Note how both Peruvian postman species *H. e. favorinus* (A) and *H. m. amaryllis* (C) show a shift in scale cell color from black to yellow, whereas the Panamanian co-mimics, *H. e. demophoon* (B) and *H. m. rosina* (D), show an extension of red patterns toward the proximal forewing with little or no yellow scale cells (light blue arrows). See also Table S1.

sampled two more co-mimetic pairs from Central America, each including an ESS and an MCS clade representative. In the co-mimetic species *H. sapho* (ESS) and *H. cydno chioneus* (MCS), loss of function of *WntA* caused different changes in pattern consistent with different underlying genetic mechanisms. The *WntA* KO in *H. sapho* was similar to *H. erato demophoon* and caused the proximal boundary of the forewing band to extend dramatically, resulting in a loss of black pattern toward the base of the forewing (Figures 2C and S4A), predicted by the proximal expression domain in larval forewings. In contrast, *H. c. chioneus* shows a much thinner *WntA* mRNA expression domain in the proximal section of the forewing that borders the discal crossvein, marking a small melanic wedge that disappears upon *WntA* KO (Figures 2D and S4B). In *H. c. chioneus*, *WntA* also affects pattern in the distal margins of both wings (Figure 2D, blue patterns in difference drawings), with the *WntA* KO showing

an increase in melanization along the distal edge of the forewing and the distal wing veins in the hindwing margins (Figures S5C and S5D), something not observed in the *H. s. sapho* co-mimic. In the latter, *WntA* affected pattern more broadly across the hindwing with an increase in melanization along its distal margin, reducing the marginal white pattern elements (Figures S5E and S5F). Further, we observed a shift from black to red scale cells across the midsection of the hindwing, which somewhat recapitulated the “*cydno C*”—a trait used to distinguish the two species in nature; remarkably, this makes the hindwing of a *H. s. sapho* *WntA* KO more closely resemble its co-mimic than in the WT state.

Perhaps the most dramatic differences in the functional effect of *WntA* KO can be seen in the two co-mimics, *H. hewitsoni* (ESS) and *H. pachinus* (MCS). In this case, we observed the loss of black across a large area of the forewing in both species. However, the specific areas where *WntA* loss of function generated pattern changes were almost opposite images of each other in some wing regions. In *H. hewitsoni*, *WntA* KO resulted

and S3). These differences were quantified in heatmaps of forewing images created by comparing the wing patterns of five WT and *WntA* KO butterflies using R/patternize [40] (Figure 2, right panels).

Additionally, we also studied the co-mimetic pair *H. e. favorinus* (ESS) and *H. m. amaryllis* (MCS) from Peru, whose postman wing patterns are very similar to *H. e. demophoon* (ESS) and *H. m. rosina* (MCS) in Panama but are geographically isolated and genetically divergent [42]. In this pair, *WntA* loss of function resulted in similar loss of black patterns to that seen in the Panamanian co-mimics, but the resulting extension of color was different (Figure 3). This was particularly true in *H. e. favorinus*, where the loss of black patterns was accompanied by an extension of yellow patterns toward the proximal forewing, something never observed in *H. e. demophoon*. In *H. m. amaryllis*, *WntA* KO caused a much more extensive shift from black to yellow scale cells than that observed in the Panamanian *melpomene* morph.

To test whether this divergence in both expression and phenotypic effects of *WntA* extends to other cases of mimicry, we



Figure 4. *WntA* Loss of Function Affects Pattern Broadly across *Heliconius* Species

(A) Phenotypes of *WntA* KO across different species of *Heliconius* within the ESS lineage (*H. e. cyrbia*, *H. charithonia*, and *H. sara*, top row) and the MCS lineage, including the silvaniforms (*H. numata*, *H. hecale melicerta*, and *H. hecale zuleika*, middle row) and *H. melpomene* and *H. cydno* (*H. m. amaryllis* and *H. cydno galanthus*). The last species in the bottom panel is *H. doris*, which falls within a third, distinct *Heliconius* lineage. As in Figure 2, the WT wing pattern is on the left and the *WntA* KO phenotype on the right. Next to each species is a schematic diagram showing the difference in pattern resulting from loss of function of *WntA* in specific wing domains. Colored areas in these drawings accentuate pattern differences in areas of the fore- and hindwing. Green color shows the loss of black patterns, yellow shows gain of black patterns, and light blue indicates gain of black patterns in distal pattern elements. The dotted gray line signals the position of *WntA* patterns across the forewing with respect to an imaginary baseline determined by the lower margin of the red forewing band in *H. erato demophoön* to show proximal and distal domains of *WntA* function.

(legend continued on next page)

in an extension of yellow through all but the apical end of the forewing (Figures 2E and S6A), whereas *WntA* KO in *H. pachinus* affected black pattern at the very distal region of the forewing, as well as from the midsection toward the proximal end of the forewing, with the exception of a few cells bordering the right margin of the discal cell (Figures 2F and S6B). Those differences in loss-of-function phenotypes are reflected by distinct *WntA* expression patterns at the larval stage: *H. hewitsoni* showed both proximal and medial expression domains that prefigure the widespread KO effects in those regions; in contrast, *H. pachinus* showed strong proximal expression, weak distal expression (both prefiguring areas of pattern shifts), and, most markedly, no expression in the median section, which was left unaffected by the KOs.

***WntA* Affects Pattern Broadly across Different Phylogenetic and Temporal Scales**

During the course of our experiments with co-mimetic pairs, we also noted important differences in the functional effects of *WntA* KO in closely related yet phenotypically different species. For example, in *H. c. chioneus*, *WntA* KO showed an increase in melanization along the distal edge of the forewing, something not observed in *H. m. rosina* *WntA* mutants. Similarly, *WntA* affected pattern more broadly across the hindwing of *H. s. sapho* than it did in the closely related but phenotypically divergent *H. e. demophoon*. These observations motivated us to explore pattern variation more broadly and determine how labile the pattern networks are across the radiation. In a sense, to answer the opposite question, “Are there any obvious limits to the role that *WntA* can play in generating pattern variation in the whole *Heliconius* group?”

To address this question, we generated *WntA* KOs in 6 additional species of *Heliconius* (Figure 1A). Across the *Heliconius* radiation, loss of function of *WntA* generated a wide array of phenotypic effects on both surfaces of the forewing and hindwing (Figure 4). In fact, knocking out *WntA* affected pattern from the base to the most distal part of both wings and both wing surfaces. This observation was true across the radiation as a whole, as well as among closely related species in the ESS and MCS lineages. Across species in the ESS lineage, which shared a common ancestor roughly 5 mya, KO of *WntA* affected pattern from the distal margin of the forewing (*H. charithonia*), across the midsection (*H. sara*), and to the most basal forewing margin (all *erato* group species; Figure 4A, top panel). On the hindwing, all ESS group species showed a pattern effect of *WntA* KO at the wing base and various species-specific pattern elements across the mid-section (*H. s. sara*), slightly more distal (*H. charithonia*), and at the hindwing margins (*H. e. cyria*; Figures S5G and S5H).

In the MCS lineage, which shared a common ancestor more recently [14], *WntA* KOs similarly affected wing patterns broadly; however, the effect of *WntA* loss of function on pattern was reduced in the proximal part of the forewing of most species relative to that seen within the ESS group (Figure 4A, bottom panel). In the silvaniforms (Figure 4A, middle panel), *WntA* loss of

function affected middle sections of the forewing, where we observed the loss of a majority of black spots against a colored background, with the exception of the lowest black spot on the discal cell (Figure 4B). Some effects of *WntA* loss of function were also observed in the marginal sections of the forewing and hindwing in this group, with variation in the size of marginal yellow and white pattern elements in *H. hecale* (Figures 4A, middle panel, S5A, and S5B).

Finally, we investigated *WntA* loss of function in *Heliconius doris*, a species that belongs to a third divergent lineage of *Heliconius* [14]. This lineage similarly contains a number of phenotypically divergent species, including ones that mimic different species in the ESS and MCS clades. *Heliconius doris* is more closely related to MCS species; yet *WntA* KO affected pattern from the base to the midsection of the forewing, more similar to the KO phenotypes seen within ESS species (Figure 4). In the ventral hindwing, we observed an increase in melanization accompanied by a reduction of red patterns radially along the red rays (Figures S5I and S5J).

***WntA* Affects Conserved and Variable Pattern Elements in a Single Species**

The discovery that *WntA* has such broad functional effects on pattern among species that shared an ancestor as little as 2.5 mya led us to investigate the extent to which *WntA* affects pattern variation within a single species of *Heliconius*. To this end, we generated *WntA* KOs for a total of 10 of the 29 color pattern morphs of *H. erato* (Figure 5). Our functional analysis included all the major wing pattern types and encompassed the entire geographic range of this species.

In all the morphs of *H. erato* investigated, *WntA* KO caused a shift in color pattern boundaries in the forewing and hindwing, with a characteristic switch from black scale cells to either red or yellow scale cells from the middle to the proximal section of the forewing (Figure 5B) and across the proximal third of the ventral hindwing (Figure 5C). Thus, there appears to be some level of conservation of the functional elements responsible for pattern variation over very recent timescales. Nonetheless, in several morphs of *H. erato*, *WntA* also affected additional pattern elements distally across the forewing and hindwing (Figure 5). For example, in *H. e. microclea*, the black band above the discal cell that breaks the forewing into two red bands is lost. Similarly, in *H. e. chestertonii* (Figures 5A and 5B), a morph that is characteristic for its fully iridescent blue/black forewing, *WntA* KO causes the reduction of black across the midsection of the wing and the appearance of red patterns. In addition, in *H. e. cyria*, *WntA* also functions in the distal margin of the hindwing to cause a switch from white to black scale cells, similar to the effect seen in the hindwing of *H. c. chioneus* (Figures 5, S5G, and S5H).

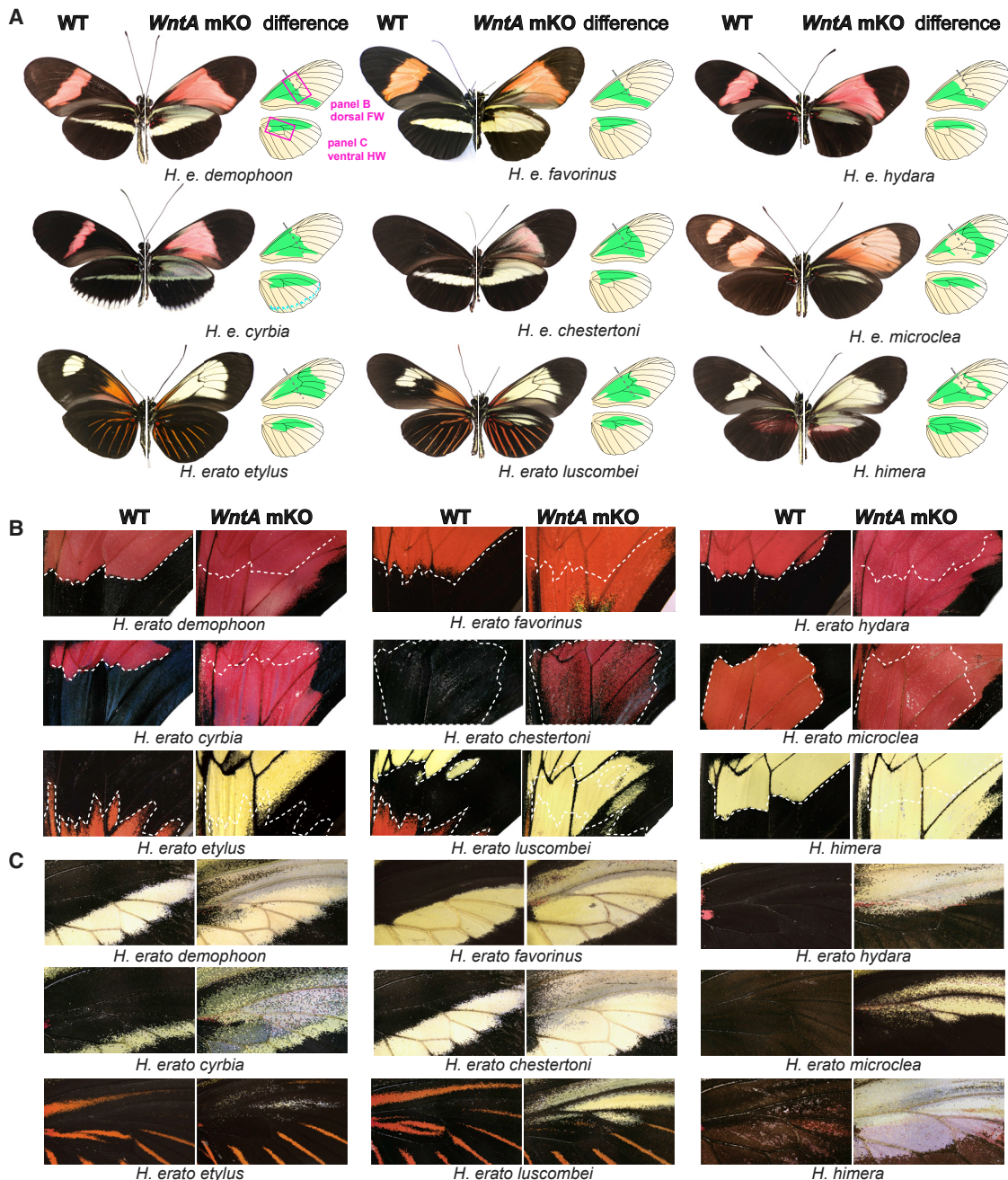
***WntA* Locally Represses *optix* to Modulate Scale Cell Color Fate**

Our *WntA* KO experiments not only revealed a very broad effect of *WntA* in generating black patterns across the whole

(B) Details of pattern elements modified by *WntA* KO across the dorsal middle to proximal forewing of WT and *WntA* KO butterflies. The dotted white lines represent the boundaries between black and color fields in the WT wing patterns.

(C) Details of pattern elements modified by *WntA* KO across the anterior ventral hindwing of WT and *WntA* KO butterflies.

For more details, see Table S1 and Figure S5.

**Figure 5. *WntA* Function across a Recent Adaptive Radiation**

(A) *WntA* loss-of-function phenotypes of nine color pattern morphs within the *H. erato* radiation. Ventral views of whole-wing phenotypes with WT wing pattern on the left and *WntA* KO on the right. Next to each species is a schematic diagram showing the difference in pattern resulting from loss of function of *WntA* in specific wing domains. Colored areas in these drawings accentuate pattern differences in areas of the fore- and hindwing. Green color shows the loss of black patterns, yellow shows gain of black patterns, and light blue indicates gain of black patterns in distal pattern elements. The dotted gray line signals the position of *WntA* patterns across the forewing with respect to an imaginary baseline determined by the lower margin of the red forewing band in *H. e. demophoon* to show proximal and distal domains of *WntA* function.

(B) Pattern differences between WT and *WntA* KO individuals in dorsal middle to proximal forewing, including the discal cell. The dotted white lines represent the boundaries between black and color fields in the WT wing patterns.

(C) Pattern differences in WT and *WntA* KO individuals across the anterior ventral hindwing.

See also Table S1 and Figure S5.

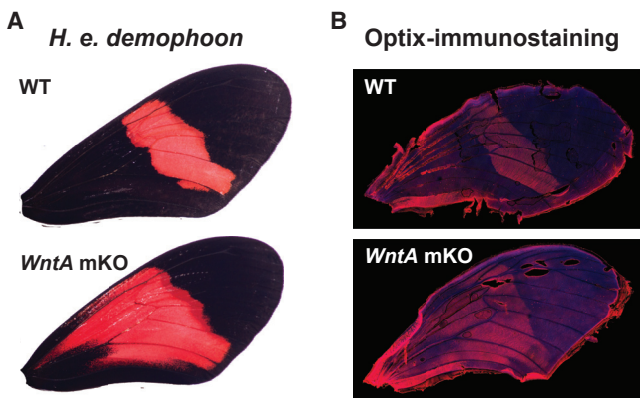


Figure 6. *WntA* Represses *optix* Expression in *Heliconius erato demophoon* Wings

WntA KO in morphs of *H. erato* that have a red forewing band results in a switch from black to red scale cells in the forewing. In *H. erato demophoon*, *WntA* loss of function and the resulting extension of red patterns from the red band toward the proximal forewing margin are correlated with an identical extension of *Optix* protein in wings sampled at 60 h post-pupation, as indicated by antibody immunostaining.

Heliconius group, but we also observed that *WntA* affects the ultimate color fate of scale cells in all possible directions. This provided us the opportunity to explore the interaction of *WntA* with *optix*, another gene involved in pattern diversity in the genus [18]. This transcription factor is both necessary and sufficient for activating red scale identity in *H. erato*, as revealed by the red-to-black aspect of *optix* CRISPR mutant clones [43] and the co-dominant effects of *optix* *cis*-regulatory alleles in *H. erato* × *H. himera* crosses [18, 29, 31]. We therefore reasoned that *WntA*, which is expressed prior to *optix* [19], could be directly or indirectly repressing *optix* to modulate red scale distribution. If our hypothesis is correct, then the expansion of red we see in our *WntA* KO of *H. e. demophoon* should correlate with an expansion of *optix* expression into the same wing domains. This was precisely the result we observed, where immunostaining of pupal wings revealed an extension of *optix* protein into the basal portion of the forewing in *WntA* mutant individuals about 60 h after pupation (Figure 6B). Thus, *WntA* is necessary for the local inhibition of *optix* in this wing area, and loss of *WntA* triggers *optix* gain of function locally, mediating a black-to-red switch in *H. e. demophoon*.

***WntA* Provides Positional Information for Scale Cell Identity**

In addition to pigment content, the chitinous ultrastructures of scales provide a second readout of scale identity. In *Heliconius* wings, scales containing a given pigment type always present the same ultrastructure [44, 45]. Given that *WntA* affects expression of *optix*, a selector gene with an important role in modulating chitinous scale cell features [43], we reasoned that *WntA* may act as an early signal that provides positional information to modulate scale cell identity. If this is true, we expected that loss of function of *WntA* would result in homeotic transformations that would affect both scale pigmentation and ultrastructure in a concomitant fashion. We tested this hypothesis in three color shifts encountered in the *H. erato* *WntA*-deficient

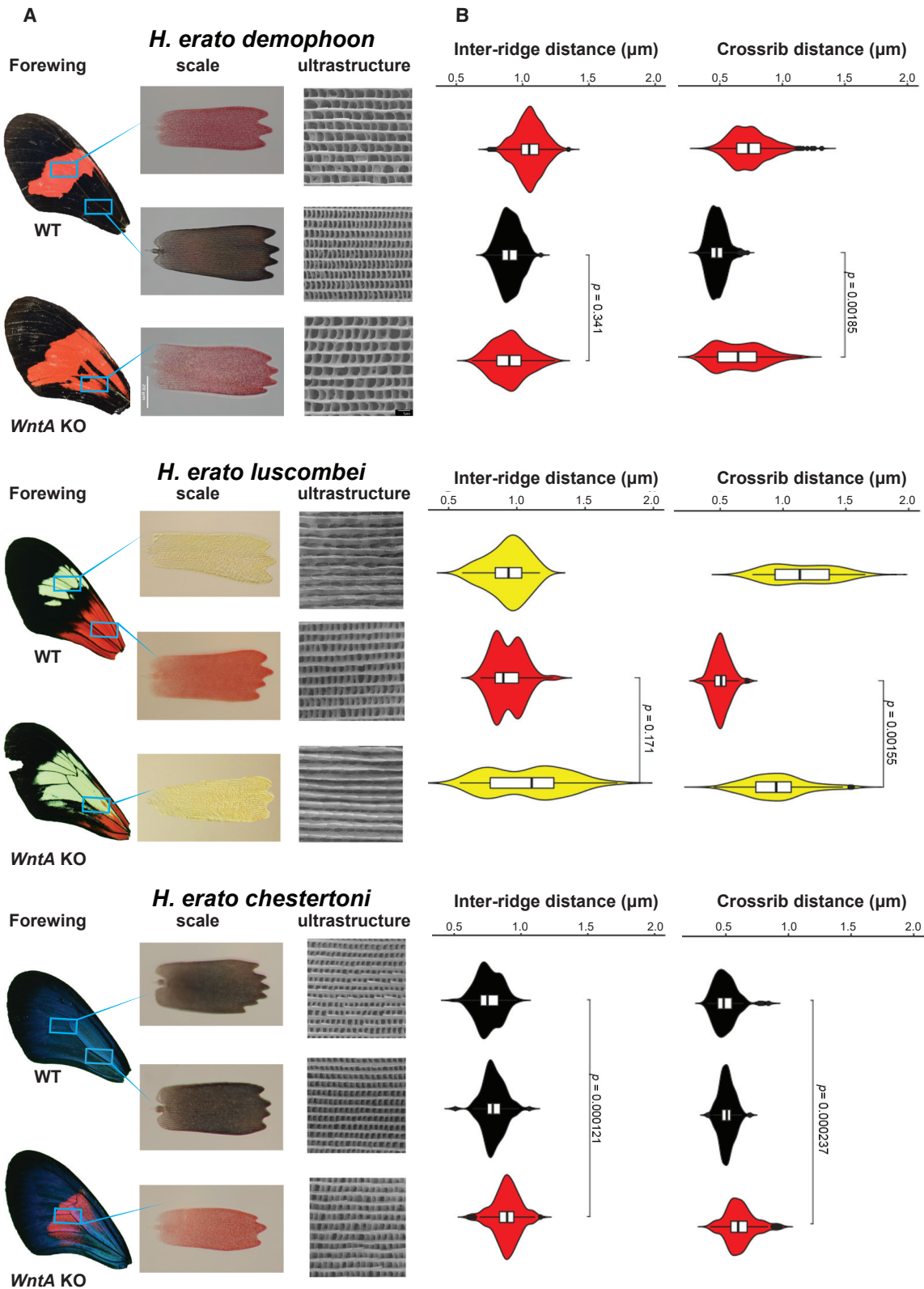
states: black to red; red to yellow; and black/blue iridescent to red (Figure 7).

There was, in fact, a shift in scale ultrastructure associated with the change in color seen in *WntA* mutants versus WTs in all three *H. erato* morphs (Figures 7A and 7B). In *H. e. demophoon*, the density of crossribs in mutant red proximal wing scale cells is much closer to WT red scale cells than to WT black proximal wing scale cells. However, this relationship did not hold for lamellar ridges (Figure 7A; see violin plots in Figure 7B). In *H. e. luscombei*, the crossrib density of mutant yellow scales from the proximal forewing was similar to the WT yellow scales of the forewing band and different from WT red scales from the proximal red patch, again signifying a homeosis of scale structure (Figure 7B). Finally, in *H. e. chestertonii*, we observed a shift in scale ultrastructure in the red scales of *WntA* KO, which presented crossrib and lamellar ridge distances that were significantly different from the black iridescent scales of the WT (Figures 7A and 7B).

Reconsidering the functional effects of *WntA* KO throughout the *Heliconius* radiation (Figure 4), it appears *WntA* is responsible for the ultimate color fate of individual scale cells. For example, in the distal section of the fore and hindwing in the silvaniform, *H. melicerta*, there was a switch from yellow to black scale cells in the yellow wing spots found along the wing margins (Figures S5A and S5B). Similar shifts to black scale cells were observed in *WntA* mutants in the forewing margins of *H. c. chioneus* and the hindwing margins of *H. s. sapho* (Figures S5C and S5F). Moreover, a number of *WntA* KOs showed a switch between red and yellow scales cells (the forewing and hindwing of *H. e. etylus* and *H. e. luscombei*; Figure 5) and a shift from red to black scale cells (for example, in the hindwing of *H. doris*; Figures 4, bottom panel, S5I, and S5J).

DISCUSSION

Steven J. Gould famously described a thought experiment as “replaying the tape of life” [46], which has provided a context for studies examining convergent evolution [1, 47]. Gould was interested in the origins of animal body plans generally and argued that there was enough inherent historical contingency to make evolutionary outcomes unpredictable; therefore, he reasoned that, if we could “replay the tape,” the results would be different. The question posited by Gould is largely a metaphysical one—the scale of life and the evolutionary process is too large for us to accurately measure through experimentation. Nonetheless, convergent evolution across branches of the tree of life does allow us to examine the tension between contingency and determinism in evolution. In the specific case of the evolution of mimetic wing patterns in *Heliconius*, which share a recent history, one might reasonably expect that the “replay” would be largely predictable, echoing the prediction by Goldschmidt that mimicry would be largely facilitated by shared genes or pathways between convergent species [48]. At some level, this is true; *WntA* affects pattern variation in all co-mimetic pairs, consistent with our recent findings that *WntA* is deeply embedded into the gene networks responsible for patterning a butterfly wing [41]. On the other hand, even across the relatively recent divergence, species evolved resemblance despite accumulated differences in their developmental landscapes.



(legend on next page)

Müllerian Mimicry across Divergent Developmental Landscapes

Müllerian mimicry is a special type of convergence, where the fitness optimum is defined by the local salience, the frequency of a warning signal, and the ability for different toxic species to converge on that pattern. In our experiments, we knocked out a key patterning locus across divergent genetic backgrounds. The KO phenotypes highlight the functional effects that this locus has on wing pattern variation and reveal considerable differences within the GRNs responsible for wing pattern convergence. In this respect, our study contributes to a growing literature that highlights how diverging genetic contexts reach convergent outputs [5–7]. The variation in pattern we observe in our KO phenotypes suggests divergence across at least three different developmental axes—(1) within the regulatory architecture surrounding *WntA* itself, (2) in the interpretation of *WntA* signaling, and (3) in other loci that play a role in patterning *Heliconius* wings. Our observation of considerable divergence in the GRNs acting on the developing wings of co-mimetic species is consistent with recent evidence from gene expression profiles of *H. e. demophoon* and *H. m. rosina*. In these experiments, the two identically patterned species showed marked variation in expression of a number of highly conserved developmental genes, including components of the Wnt signaling pathway and many transcription factors during early wing development [49]. This rapid divergence is reminiscent of changes in the GRNs responsible for generating eyespots patterns in nymphalid butterflies [13] or underpinning many phenotypic similarities between closely related nematode species [50].

Rapid Change in *WntA* Regulatory Landscape

At the most basic level, our KO experiments reveal a great degree of variability in where *WntA* is expressed in developing *Heliconius* butterflies. This variation was evident in the different patterns of mRNA expression observed in co-mimetic pairs (Figure 2), in previous studies reporting highly variable and pattern-specific *WntA* expression across *Heliconius* species [30], and in the broad range of phenotypic effects uncovered in our *WntA* KO phenotypes. It is instructive to cast the role that *WntA* plays in pattern variation in *Heliconius* relative to the role that this locus plays in pattern variation across the hyper-diverse nymphalid lineage—a group of over 6,000 species of butterflies, including *Heliconius*. Across the nymphalids, which diverged from a common ancestor roughly 65 mya, *WntA* has been extensively rewired and repurposed to affect a wide variety of pattern elements [41], including determining scale cell types along the wing margins, across the central region of both wings, as well as within the more proximal sections of both wings. *Heliconius* shows a similar regulatory flexibility but over much more recent timescales. For example, in species that shared a common ancestor within the last 3.5–6.5 Ma, *WntA* affects pattern variation across both wing surfaces from the wing tips to the wing base and shifts the ultimate color and structural fate of a wing scale cell in every possible direction (see Figures 4, 5, and S5).

Our loss-of-function evidence complements recent genotype-phenotype analyses of *H. erato* morphs that differed in the size, shape, and position of the forewing band, which pinpoint the causal roles of *cis*-regulatory (non-coding) regions around *WntA* in forging pattern shape variation across the midsection of the forewing [36]. Similarly, our *WntA* KO experiments across the same suite of *H. erato* morphs resulted in pattern boundary shifts across the midsection of the forewing, consistent with the effects of a number of different *cis*-regulatory alleles in this region (Figure 5). Overall, the combination of mapping, expression, and functional experiments conducted in the *Heliconius* group reveals that the upstream regulation of *WntA* expression varies substantially between closely related species that have very different wing patterns, as well as between distantly related, yet identically patterned, co-mimic pairs.

WntA Is a Pre-patterning Gene that Controls Wing Scale Cell Identity

The diversity of KO effects emphasizes the key role that *WntA* plays in determining scale cell fate. Indeed, *WntA* KO not only affected scale cell pigmentation but also caused a homeotic shift in scale cell ultrastructure. We use a broad definition for the term “homeotic” here, which refers to the “assumption of one part of an organism to likeness of another part” [51]. This definition applies in this case because loss of function of *WntA* causes a wing scale cell to change its identity and fully acquire the identity of a different kind of scale cell, revealing a fundamental role of *WntA* in the developmental process that leads to the establishment of scale cell fate. This fundamental role of *WntA* is illustrated in the observation that the shift in scale cell fate happens in every possible direction, from black to red, yellow, and white, as well as from color to black, and also from red to yellow scales. Thus, we conclude that *WntA* ligands provide key positional context for the downstream expression of a variety of selector genes that determine scale cell color and ultrastructure across the wing.

We show that the ultimate color and structural fate of a scale cell is highly context dependent, suggesting that *WntA* interacts with downstream wing patterning pathways in complex ways, generating another hierarchical level at which wing patterning networks diverge. The complexity of these interactions is best demonstrated in the different responses of *optix* to *WntA* KO in divergent color pattern morphs of *H. erato*. In some genetic contexts, *WntA* KO results in an upregulation of *optix* (Figure 6). However, the opposite is true in yellow-banded morphs of *H. erato* (e.g., compare rows 1 and 2 versus row 3 in Figure 5A), where KO results in a shift to yellow scales, even across the red patch, which is known to express *optix* in non-mutant butterflies [18]. We speculate that this expansion of proximal forewing yellow, observed throughout both the ESS and MCS clades (Figures 4 and 5), may be due to direct or indirect roles of *WntA* signaling in representing one or several yellow-associated selector genes that remain to be discovered. Connections between *WntA* signals and other

Figure 7. Scale Ultrastructure Shifts in WT and *WntA* KO Dorsal Forewings

(A) Images showing scale cell shape and ultrastructure in WT and *WntA* KO dorsal forewings of *H. e. demophoon*, *H. e. etylus*, and *H. e. chestertonii*, across the region of mutant change from the middle to the proximal forewing margins.
 (B) Violin plots of measurements of scale ultrastructure elements: crossrib distance and inter-ridge distance, with corresponding statistical analysis shown on top of each figure. *WntA* KO affects scale cell ultrastructure in black, red, and yellow scales, consistent with homeosis in scale cell identity.

downstream loci are extremely labile, and even in phenotypically similar yet allopatric red-banded morphs of *H. erato* and *H. melpomene*, there were within-species differences in how scale cells responded to the loss of *WntA* signals (Figure 3).

Hidden Variation in Patterning Networks

Finally, *WntA* mutants expose underlying differences in the expression of other patterning loci that influence pattern matching. The observation is perhaps best exemplified in the functional KO of *WntA* in *H. hewitsoni* (ESS) and *H. pachinus* (MCS) (Figures 2E and 2F), where the large melanic patches that make up the mimetic forewing patterns are under different genetic control, with *WntA* affecting pattern distally in *H. pachinus*, but not in *H. hewitsoni*; across the midsection of the forewing in *H. hewitsoni*, but not *H. pachinus*; and in the most proximal section of the forewing in *H. hewitsoni*, but not *H. pachinus*. Thus, other loci are also responsible for aspects of black patterning in *Heliconius*. This observation is completely consistent with decades of crossing experiments, where black patterning is also modulated by cortex (see [35] for a recent example in MCS group species). Moreover, in other butterflies, including *Agraulis vanillae*, *Euphydryas chalcedona*, and *Vanessa cardui*, several members of the Wnt pathway of signaling ligands appear to contribute to creating black patterns [52]. This may also be the case in *Heliconius*, although the individual contributions of other Wnt signaling ligands to wing patterning have not yet been tested.

This complementarity of gene function may explain the differences in *WntA* mKO effects observed between ESS and MCS species. For example, note the subtle phenotypic effects of *WntA* KO in the median region of *H. melpomene rosina* forewings (Figure 2B), in spite of intense *WntA* mRNA detection in that area. In this case, removing *WntA* only causes a subtle shift of the distal boundary of the red band instead of drastically expanding this pattern, as would be expected from the co-mimic *H. e. demophoon*. Other genes are likely to be functional in this wing domain that may mitigate the requirement of a single signal to properly establish the pattern boundary. Similar to *WntA*, these genes are expected to be deployed differently among co-mimic pairs, providing an additional source of variation for natural selection to act upon and additional paths to the evolution of convergent phenotypes.

In conclusion, co-mimetic *Heliconius* pairs last shared a common ancestor roughly 10–14 mya and converged on similar wing pattern phenotypes within the last 2.5–4.5 Ma. Our *WntA* loss-of-function experiments demonstrate that, over the relatively short time periods in which species of the two clades were evolving independently, the pathways involved in developing wing patterns diverged substantially and natural selection drove the evolution of convergent wing patterns differently. In this sense, evolution is predictable, as *WntA* is always being used to generate pattern variation. However, the gene is being used in very different ways. Divergence in the expression of *WntA*, in how loci respond to *WntA* signals, and other complementary patterning pathways all contribute to create differences in the gene networks that pattern the wing in co-mimetic pairs. We show that this divergence opens additional contingencies and creates extraordinary flexibility for natural selection to drive the rapid evolution of highly convergent wing patterns in fantastic and unpredictable ways.

STAR★METHODS

Detailed methods are provided in the online version of this paper and include the following:

- KEY RESOURCES TABLE
- LEAD CONTACT AND MATERIALS AVAILABILITY
- EXPERIMENTAL MODEL AND SUBJECT DETAILS
- METHOD DETAILS
 - CRISPR/Cas9 genome editing
 - Genotyping mutants with deep sequencing
 - *In situ* Hybridizations
 - Immunofluorescence
- QUANTIFICATION AND STATISTICAL ANALYSIS
 - Automated image analysis of clonal mutant butterflies
 - Quantitative analysis of wing scale morphology and ultrastructure
- DATA AND CODE AVAILABILITY

SUPPLEMENTAL INFORMATION

Supplemental Information can be found online at <https://doi.org/10.1016/j.cub.2019.10.010>.

ACKNOWLEDGMENTS

We thank Oscar Paneso, Cruz Batista, Lissette Rivera, Lissette Jimenez, and Clement Aubert for technical support with rearing of butterfly stocks and larvae resulting from experimental procedures. We are also grateful to Krzysztof “Chris” Kozak, Michael Logan, and Eric Haag for thoughtful discussions and feedback on the manuscript. We thank Robert Reed for sharing anti-optix antibodies to produce pupal wing immunostainings and to Sebastian Mena for taking professional photo images of mutant and WT butterflies. This research was funded by a Smithsonian Institute Pell Grant to W.O.M.; Smithsonian Institute Scholarly Studies Award to W.O.M. and C.C.; Smithsonian Institute Biodiversity Genomics Fellowship Award to C.C.; the National Science Foundation awards IOS-1656553 and IOS-1755329 to A.M.; National Science Foundation awards IOS-1656389 to R.P. and OIA 1736026 to B.C. and R.P.; funds from Universidad del Rosario for M.L., C.P.-D., and C.S.; and a Leverhulme Trust project grant RPG-2014-167 to C.D.J. We would like to dedicate this article to the memory of Sabrina Ferrara, who was an intern in our team and died before she could see the publication of this work. She was a kind person, and we remember her with affection.

AUTHOR CONTRIBUTIONS

Conceptualization, C.C. and W.O.M.; Methodology, C.C., A.M., M.J.S., and D.F.P.; Investigation, C.C., R.W.R.W., J.J.H., J. Fenner, L.L., E.S.R., D.F.P., C.A., M.V., M.S., C.M., D.T., C.P.-D., P.A., S.F., J. Foley, and D.M.; Writing – Original Draft, C.C. and W.O.M.; Writing – Review & Editing, W.O.M., A.M., J.J.H., R.P., C.D.J., L.L., B.A.C., C.P.-D., C.S., M.L., and J. Fenner; Funding Acquisition, W.O.M., C.C., A.M., R.P., C.D.J., and B.A.C.; Resources, W.O.M. and A.M.; Supervision, W.O.M. and A.M.

DECLARATION OF INTERESTS

The authors declare no competing interests.

Received: July 9, 2019

Revised: August 26, 2019

Accepted: October 8, 2019

Published: November 14, 2019

REFERENCES

- Blount, Z.D., Lenski, R.E., and Losos, J.B. (2018). Contingency and determinism in evolution: replaying life's tape. *Science* 362, eaam5979.
- Haag, E.S., and True, J.R. (2001). Perspective: from mutants to mechanisms? Assessing the candidate gene paradigm in evolutionary biology. *Evolution* 55, 1077–1084.
- Kratochwil, C.F., Liang, Y., Gerwin, J., Woltering, J.M., Urban, S., Henning, F., Machado-Schiaffino, G., Hulsey, C.D., and Meyer, A. (2018). Agouti-related peptide 2 facilitates convergent evolution of stripe patterns across cichlid fish radiations. *Science* 362, 457–460.
- True, J.R., and Haag, E.S. (2001). Developmental system drift and flexibility in evolutionary trajectories. *Evol. Dev.* 3, 109–119.
- Kittelmann, S., Buffry, A.D., Franke, F.A., Almudi, I., Yoth, M., Sabaris, G., Couso, J.P., Nunes, M.D.S., Frankel, N., Gómez-Skarmeta, J.L., et al. (2018). Gene regulatory network architecture in different developmental contexts influences the genetic basis of morphological evolution. *PLoS Genet.* 14, e1007375.
- Sorrells, T.R., Johnson, A.N., Howard, C.J., Britton, C.S., Fowler, K.R., Feigerle, J.T., Weil, P.A., and Johnson, A.D. (2018). Intrinsic cooperativity potentiates parallel *cis*-regulatory evolution. *eLife* 7, 37563.
- Ellison, C., and Bachtrog, D. (2019). Contingency in the convergent evolution of a regulatory network: Dosage compensation in *Drosophila*. *PLoS Biol.* 17, e3000094.
- Nijhout, H.F. (1991). *The Development and Evolution of Butterfly Wing Patterns* (Smithsonian Institution Press).
- Bates, H.W. (1862). XXXII: contributions to an insect fauna of the Amazon valley (Lepidoptera: Heliconidae). *Trans. Linn. Soc. London* 23, 495–566.
- Müller, F. (1879). Ituna and Thyridia; a remarkable case of mimicry in butterflies. *Trans. Ent. Soc. Lond.* 20–29.
- Scotland, R.W. (2011). What is parallelism? *Evol. Dev.* 13, 214–227.
- Espeland, M., Breinholt, J., Willmott, K.R., Warren, A.D., Vila, R., Toussaint, E.F.A., Maunsell, S.C., Aduse-Poku, K., Talavera, G., Eastwood, R., et al. (2018). A comprehensive and dated phylogenomic analysis of butterflies. *Curr. Biol.* 28, 770–778.e5.
- Oliver, J.C., Tong, X.-L., Gall, L.F., Piel, W.H., and Monteiro, A. (2012). A single origin for nymphalid butterfly eyespots followed by widespread loss of associated gene expression. *PLoS Genet.* 8, e1002893–e1002898.
- Kozak, K.M., Wahlberg, N., Neild, A.F.E., Dasmahapatra, K.K., Mallet, J., and Jiggins, C.D. (2015). Multilocus species trees show the recent adaptive radiation of the mimetic *Heliconius* butterflies. *Syst. Biol.* 64, 505–524.
- Turner, J.R.G. (1981). Adaptation and evolution in *Heliconius*: a defense of NeoDarwinism. *Annu. Rev. Ecol. Syst.* 12, 99–121.
- Brown, K.S. (1981). The biology of *Heliconius* and related genera. *Annu. Rev. Entomol.* 26, 427–457.
- Mallet, J. (1993). Speciation, ratiation, and color pattern evolution in *Heliconius* butterflies: evidence from hybrid zones. In *Hybrid Zones and the Evolutionary Process*, R.G. Harrison, ed. (Oxford University), pp. 226–260.
- Reed, R.D., Papa, R., Martin, A., Hines, H.M., Counterman, B.A., Pardo-Diaz, C., Jiggins, C.D., Chamberlain, N.L., Kronforst, M.R., Chen, R., et al. (2011). *optix* drives the repeated convergent evolution of butterfly wing pattern mimicry. *Science* 333, 1137–1141.
- Martin, A., Papa, R., Nadeau, N.J., Hill, R.I., Counterman, B.A., Halder, G., Jiggins, C.D., Kronforst, M.R., Long, A.D., McMillan, W.O., and Reed, R.D. (2012). Diversification of complex butterfly wing patterns by repeated regulatory evolution of a *Wnt* ligand. *Proc. Natl. Acad. Sci. USA* 109, 12632–12637.
- Nadeau, N.J., Pardo-Diaz, C., Whibley, A., Supple, M.A., Saenko, S.V., Wallbank, R.W.R., Wu, G.C., Maroja, L., Ferguson, L., Hanly, J.J., et al. (2016). The gene *cortex* controls mimicry and crypsis in butterflies and moths. *Nature* 534, 106–110.
- Westerman, E.L., VanKuren, N.W., Massardo, D., Tenger-Trolander, A., Zhang, W., Hill, R.I., Perry, M., Bayala, E., Barr, K., Chamberlain, N., et al. (2018). *Aristaless* controls butterfly wing color variation used in mimicry and mate choice. *Curr. Biol.* 28, 3469–3474.e4.
- Beltrán, M., Jiggins, C.D., Brower, A.V.Z., Bermingham, E., and Mallet, J. (2007). Do pollen feeding, pupal-mating and larval gregariousness have a single origin in *Heliconius* butterflies? Inferences from multilocus DNA sequence data. *Biol. J. Linn. Soc. Lond.* 92, 221–239.
- Jiggins, C.D. (2017). *The Ecology and Evolution of Heliconius Butterflies*, First Edition (Oxford University Press).
- McCulloch, K.J., Yuan, F., Zhen, Y., Aardema, M.L., Smith, G., Llorente-Bousquets, J., Andolfatto, P., and Briscoe, A.D. (2017). Sexual dimorphism and retinal mosaic diversification following the evolution of a violet receptor in butterflies. *Mol. Biol. Evol.* 34, 2271–2284.
- Kozak, K.M., McMillan, W.O., Joron, M., and Jiggins, C.D. (2018). Genome-wide admixture is common across the *Heliconius* radiation. *bioRxiv*. <https://doi.org/10.1101/414201>.
- Edelman, N.B., Frandsen, P.B., Miyagi, M., Clavijo, B., Davey, J., Dikow, R., Garcia-Accinelli, G., van Belleghem, S., Patterson, N., Neafsey, D.E., et al. (2018). Genomic architecture and introgression shape a butterfly radiation. *bioRxiv*. <https://doi.org/10.1101/466292>.
- Bolognesi, R., Farzana, L., Fischer, T.D., and Brown, S.J. (2008). Multiple *Wnt* genes are required for segmentation in the short-germ embryo of *Tribolium castaneum*. *Curr. Biol.* 18, 1624–1629.
- Jiggins, C.D., Mavárez, J., Beltrán, M., McMillan, W.O., Johnston, J.S., and Bermingham, E. (2005). A genetic linkage map of the mimetic butterfly *Heliconius melpomene*. *Genetics* 171, 557–570.
- Kapan, D.D., Flanagan, N.S., Tobler, A., Papa, R., Reed, R.D., Gonzalez, J.A., Restrepo, M.R., Martinez, L., Maldonado, K., Ritschoff, C., et al. (2006). Localization of Müllerian mimicry genes on a dense linkage map of *Heliconius erato*. *Genetics* 173, 735–757.
- Martin, A., Papa, R., Nadeau, N.J., Hill, R.I., Counterman, B.A., Halder, G., Jiggins, C.D., Kronforst, M.R., Long, A.D., McMillan, W.O., et al. (2012). Diversification of complex butterfly wing patterns by repeated regulatory evolution of a *Wnt* ligand. *Proc. Natl. Acad. Sci. USA* 109, 12632–12637.
- Papa, R., Kapan, D.D., Counterman, B.A., Maldonado, K., Lindstrom, D.P., Reed, R.D., Nijhout, H.F., Hrbek, T., and McMillan, W.O. (2013). Multi-allelic major effect genes interact with minor effect QTLs to control adaptive color pattern variation in *Heliconius erato*. *PLoS ONE* 8, e57033.
- Baxter, S.W., Johnston, S.E., and Jiggins, C.D. (2009). Butterfly speciation and the distribution of gene effect sizes fixed during adaptation. *Heredity* 102, 57–65.
- Huber, B., Whibley, A., Poul, Y.L., Navarro, N., Martin, A., Baxter, S., Shah, A., Gilles, B., Wirth, T., McMillan, W.O., and Joron, M. (2015). Conservatism and novelty in the genetic architecture of adaptation in *Heliconius* butterflies. *Heredity* 114, 515–524.
- Gallant, J.R., Imhoff, V.E., Martin, A., Savage, W.K., Chamberlain, N.L., Pote, B.L., Peterson, C., Smith, G.E., Evans, B., Reed, R.D., et al. (2014). Ancient homology underlies adaptive mimetic diversity across butterflies. *Nat. Commun.* 5, 4817.
- Morris, J., Navarro, N., Rastas, P., Rawlins, L.D., Sammy, J., Mallet, J., and Dasmahapatra, K.K. (2019). The genetic architecture of adaptation: convergence and pleiotropy in *Heliconius* wing pattern evolution. *Heredity* 123, 138–152.
- Van Belleghem, S.M., Rastas, P., Papanicolaou, A., Martin, S.H., Arias, C.F., Supple, M.A., Hanly, J.J., Mallet, J., Lewis, J.J., Hines, H.M., et al. (2017). Complex modular architecture around a simple toolkit of wing pattern genes. *Nat. Ecol. Evol.* 1, 52.
- Martin, A., and Courtier-Orgogozo, V. (2017). Diversity and evolution of butterfly wing patterns. In *Morphological Evolution Repeatedly Caused by Mutation in Signaling Ligand Genes*, T. Sekimura, and H.F. Nijhout, eds. (Springer Singapore), pp. 1–54.
- Doudna, J.A., and Charpentier, E. (2014). Genome editing. The new frontier of genome engineering with CRISPR-Cas9. *Science* 346, 1258096.
- Livraghi, L., Martin, A., Gibbs, M., Braak, N., Arif, S., and Breuker, C.J. (2018). CRISPR/Cas9 as the key to unlocking the secrets of butterfly

- wing pattern development and its evolution. *Adv. Insect Physiol.* 54, 85–115.
40. Van Belleghem, S.M., Papa, R., Ortiz-Zuazaga, H., Hendrickx, F., Jiggins, C.D., McMillan, W.O., and Counterman, B.A. (2018). patternize: an R package for quantifying colour pattern variation. *Methods Ecol. Evol.* 9, 390–398.
 41. Mazo-Vargas, A., Concha, C., Livraghi, L., Massardo, D., Wallbank, R.W.R., Zhang, L., Papador, J.D., Martinez-Najera, D., Jiggins, C.D., Kronforst, M.R., et al. (2017). Macroevolutionary shifts of *WntA* function potentiate butterfly wing-pattern diversity. *Proc. Natl. Acad. Sci. USA* 114, 10701–10706.
 42. Hines, H.M., Counterman, B.A., Papa, R., Albuquerque de Moura, P., Cardoso, M.Z., Linares, M., Mallet, J., Reed, R.D., Jiggins, C.D., Kronforst, M.R., et al. (2011). Wing patterning gene redefines the mimetic history of *Heliconius* butterflies. *Proc. Natl. Acad. Sci. USA* 108, 19666–19671.
 43. Zhang, L., Mazo-Vargas, A., and Reed, R.D. (2017). Single master regulatory gene coordinates the evolution and development of butterfly color and iridescence. *Proc. Natl. Acad. Sci. USA* 114, 10707–10712.
 44. Gilbert, L.E., Forrest, H.S., Schultz, T.D., and Harvey, D.J. (1988). Correlations of ultrastructure and pigmentation suggest how genes control development of wing scales of *Heliconius* butterflies. *J. Res. Lepid.* 26, 141–160.
 45. Janssen, J.M., Monteiro, A., and Brakefield, P.M. (2001). Correlations between scale structure and pigmentation in butterfly wings. *Evol. Dev.* 3, 415–423.
 46. Gould, S.J. (1990). *Wonderful Life: The Burgess Shale and the History of Nature* (WW Norton & Company).
 47. Powell, R., and Mariscal, C. (2015). Convergent evolution as natural experiment: the tape of life reconsidered. *Interface Focus* 5, 20150040.
 48. Goldschmidt, R.B. (1945). Mimetic polymorphism, a controversial chapter of Darwinism. *Q. Rev. Biol.* 20, 205–230.
 49. Hanly, J.J., Wallbank, R.W.R., McMillan, W.O., and Jiggins, C.D. (2019). Conservation and flexibility in the gene regulatory landscape of heliconiine butterfly wings. *Evodevo* 10, 15.
 50. Verster, A.J., Raman, A.K., McKay, S.J., and Fraser, A.G. (2014). Comparative RNAi screens in *C. elegans* and *C. briggsae* reveal the impact of developmental system drift on gene function. *PLoS Genet.* 10, e1004077.
 51. Leavitt, R.G. (1909). A vegetative mutant, and the principle of homoeosis in plants. *Bot. Gaz.* 47, 30–68.
 52. Martin, A., and Reed, R.D. (2014). Wnt signaling underlies evolution and development of the butterfly wing pattern symmetry systems. *Dev. Biol.* 395, 367–378.
 53. Bassett, A., and Liu, J.-L. (2014). CRISPR/Cas9 mediated genome engineering in *Drosophila*. *Methods* 69, 128–136.
 54. Margam, V.M., Gachomo, E.W., Shukle, J.H., Ariyo, O.O., Seufferheld, M.J., and Kotchoni, S.O. (2010). A simplified arthropod genomic-DNA extraction protocol for polymerase chain reaction (PCR)-based specimen identification through barcoding. *Mol. Biol. Rep.* 37, 3631–3635.
 55. Bolger, A.M., Lohse, M., and Usadel, B. (2014). Trimmomatic: a flexible trimmer for Illumina sequence data. *Bioinformatics* 30, 2114–2120.
 56. Liu, B., Yuan, J., Yiu, S.-M., Li, Z., Xie, Y., Chen, Y., Shi, Y., Zhang, H., Li, Y., Lam, T.-W., and Luo, R. (2012). COPE: an accurate k-mer-based pair-end reads connection tool to facilitate genome assembly. *Bioinformatics* 28, 2870–2874.
 57. Rice, P., Longden, I., and Bleasby, A. (2000). EMBOSS: the European Molecular Biology Open Software Suite. *Trends Genet.* 16, 276–277.
 58. Pinello, L., Canver, M.C., Hoban, M.D., Orkin, S.H., Kohn, D.B., Bauer, D.E., and Yuan, G.-C. (2016). Analyzing CRISPR genome-editing experiments with CRISPResso. *Nat. Biotechnol.* 34, 695–697.

STAR★METHODS**KEY RESOURCES TABLE**

REAGENT or RESOURCE	SOURCE	IDENTIFIER
Antibodies		
Optix antibodies	Robert Reed Lab, Cornell University	N/A
anti- rat IgG Alexa488	Cell Signaling Technology	4416S
Chemicals, Peptides, and Recombinant Proteins		
Cas9 protein	PNABio	CP01200
Primers (desalted)	IDT	https://www.idtdna.com/pages
KAPA Pure Beads	Roche	07983280001
Platinum Hotstart PCR Master Mix	Thermofisher	13000012
Critical Commercial Assays		
T7 MEGAshortscript kit	Invitrogen	AM1354
PCR cleanup kit	QIAGEN	28104
Phusion High Fidelity PCR kit	New England Biolabs	E0553L
pGEMt easy vector	Promega	A1360
Software and Algorithms		
FastQC v0.11.7	http://www.bioinformatics.babraham.ac.uk/projects/fastqc/	N/A
Trimmomatic v0.38	http://www.usadellab.org/cms/?page=trimmomatic	N/A
COPE v1.2.5	https://github.com/dhlbh/COPE	N/A
CRISPResso	https://github.com/lucapinello/CRISPResso	N/A
WntA KO patternize	https://github.com/Hanlonius	N/A
Violin plot software	https://CRAN.R-project.org/package=ggplot2	N/A
Statistical analysis software	https://CRAN.R-project.org/package=ggpubr	N/A

LEAD CONTACT AND MATERIALS AVAILABILITY

Further information and requests for resources, such as access to butterfly stocks and insectary and laboratory space in STRI Gamboa, Panama, should be directed to and will be fulfilled by the senior author, Owen McMillan at mcmillano@si.edu. This work didn't generate any new reagents.

EXPERIMENTAL MODEL AND SUBJECT DETAILS

Heliconius butterflies were collected from the field in Pipeline Road in Gamboa, Panama, in the Tarapoto region in Peru, in the Macas and Puyo region in Ecuador and in the Cauca Valley in Colombia by members of our team. Stocks of butterflies were reared and maintained at the outdoor insectaries of the Smithsonian Tropical Research Institute in Gamboa, Panama with Smithsonian Institution permission for animal care and in insectaries in La Vega, Colombia. For regular maintenance, adults were kept in big outdoor net cages of 3 m high by 3 × 3 m at the base, with a protective roof to shield from the rain, containing abundant nectary plants for adult feeding, including *Psiguria* and *Psychotria*. The rearing temperatures ranged between 28–32°C and humidity ranged between 70%–85% depending on the season. Butterflies were also fed daily a mix of sugar water and pollen and given fresh *Psiguria* and *Lantana* flowers as an additional protein source. Females were given specific *Passiflora* hostplants for egg laying, depending on the species, and larvae were reared on big plants or on large shoots cut from the plants and placed in bottles with water, protected from parasites and predators within a small tabletop net cage, until they pupated. The necessary butterfly collection permits were obtained from the governments of each country and importation permits were obtained from the Ministry of the Environment of Panama, according to the Panamanian Government and STRI regulations. Rearing and experimentation complied with local government regulations on containment and handling.

METHOD DETAILS

CRISPR/Cas9 genome editing

In order to perform the targeted mutagenesis of the *WntA* gene, we first made a multiple sequence alignment that included the coding sequence for *WntA* of several species and morphs of *Heliconius* butterflies. Using this alignment, we selected the most conserved regions for designing our targeting strategy. Two gRNA were designed against the second coding exon of the *WntA* gene by searching for sequences that had GG before the PAM motif (N₁₈NNG): W1: ACAGACAGGTGCTAACAGG and W2: AACAGCACTGATA TATTTGG. These sequences were tested for uniqueness by BLASTing them against the *H. erato* genome [36]. DNA templates for gRNA synthesis were obtained by PCR using Phusion polymerase (NEB), purified with the PCR cleanup kit (QIAGEN) and quantified with nanodrop. Subsequently, gRNAs were synthesized using the T7 MEGAshortscript kit (Ambion) according to the protocol by Bassett and Liu [53].

For targeted mutagenesis of *Heliconius* embryos, a mix of gRNA and Cas9 protein (PNA Bio) 300:500 µg/µl was microinjected into syncytial *Heliconius* embryos between 1-3 h after egg laying using a Sutter Instruments Xenoworks microinjector and quartz needles made using a Sutter instruments P2000 needle puller. Embryos were individually reared to adulthood in plastic cups at 25°C and 70% humidity, and G₀ butterflies were observed for mutant phenotypes. For genotyping, genomic DNA was obtained from butterfly legs using the protocol by Margam and collaborators [54]. A 400 bp DNA fragment that spans the target site was amplified by PCR using primers that bind to intronic regions at either side of the *WntA* second exon: F2: CCTCAGTCAGTCAGCACAAAGCC and R2: CTCAA GAAGCCAAGTAGTAAAGTG. PCR products were either cloned into the pGEMt easy vector and sequenced by Sanger (data not shown) or used for Illumina deep sequencing.

Genotyping mutants with deep sequencing

To obtain a broader view of the mutations caused by CRISPR/Cas9 in the adult butterflies and the differences between fully symmetric and mosaic phenotypes we performed deep sequencing of a PCR product amplified from wild-type, mutant and non mutant injected butterflies (Figures S1 and S2 and Table S2). A region spanning the CRISPR cutting site was amplified using a 2-step PCR protocol. The first PCR used primers *WntA*-illuminaseq-F2: CACTCTTCCCTACACGACGCTCTCCGATCTCCTCAGTCAGTCAG CACAAAGCC and *WntA*-illuminaseqR2: GTGACTGGAGTTCAGACGTGCTCTCCGATCTCAAGAAGCCAAGTAGTAAGTG and was performed in 25 µL final volume. The PCR mix contained: 0.2 µM of each primer, 200 µM dNTPs, 1X PCR buffer, 1.5 nM MgCl₂, 0.5 µL DMSO, 0.5U Phusion High-Fidelity DNA Polymerase (NEB), and 1 µL DNA template. Cycling conditions were 2' at 98°C, followed by 30 cycles of 30" at 98°C, 30" at 49°C and 45" at 72°C, with a final extension of 5' at 72°C. PCR products were then cleaned using 1X volume KAPApure beads (Roche) following manufacturer procedure. A second PCR was then performed to add the Illumina flow cell binding sequences and an 8nt barcode to identify each sample, using 5 µL Platinum Hot Start PCR Master Mix (ThermoFisher), 1 µL each Illumina primer and 2ul clean PCR product in a 11.5 µL reaction. Cycling conditions were 2" at 94°C, followed by 8 cycles of 45" at 94°C, 60" at 50°C and 90" at 72°C, with a final extension of 10' at 72°C. PCR products were quantified using a Qubit fluorometer (ThermoFisher), pooled equimolarly and then cleaned using 1X volume KAPApure beads (Roche). The pooled library was sequenced on an Illumina MiSeq using 250 PE on a 500 cycle V2 kit. Raw reads were checked for their qualities with FastQC v0.11.7 (<http://www.bioinformatics.babraham.ac.uk/projects/fastqc/>), and then cleaned up for Illumina adapters and low quality regions (Q < 20) using Trimmomatic v0.38 [55]. Overlapping pair-end cleaned reads were then connected using COPE v1.2.5 [56]. The resulting joined reads were aligned to the wild-type *WntA* reference sequence with Needle, from the EMBOSS suite [57], and examined for the presence of indels using the pipeline CRISPResso [58].

In situ Hybridizations

To complement our *WntA* loss of function experiments we performed *in situ* hybridizations to observe the distribution of *WntA* mRNA in wild-type developing wing discs (Figure 2). Fifth-instar larvae were anaesthetized on ice for ten minutes and then dissected in cold Phosphate Buffer Solution 1x (PBS) to obtain the wing discs. Wing discs were incubated in cold fixative (formaldehyde 9.25% in PBS containing 50 mM EGTA) for 30-35 min, followed by five rinses in PBS with 0.01% Tween20 (PBST) for 3 minutes each time and then incubated with 25 µg/mL proteinase K in cold PBST for 5 minutes. To stop the proteinase K reaction, wing discs were washed in cold PBST containing 2mg/mL glycine for 5 minutes, then washed twice in cold PBST and freed from their peripodial membrane using fine forceps. The tissues were then post-fixed 20min on ice in PBS containing 5.5% formaldehyde, followed by five washes in cold PBST for 3 minutes each, and transferred to a standard hybridization buffer (5X saline sodium citrate pH 4.5, 50% formamide, 0.01% Tween20, 100 µg/mL denatured salmon sperm DNA, final pH 5-6) that was placed at 62°C for an hour. To start the labeling process, tissues were then incubated in hybridization buffer supplemented with 1 g/L glycine and 30-50 ng/mL riboprobe for 16-40h at 62°C. Wing discs were then washed eight times for 15-30 min in hybridization buffer, returned to room temperature, and gradually stepped back into PBST. For secondary detection of the riboprobe, the tissues were blocked for 30 min in Tris buffer saline, 0.01% Tween20 (TBST, pH = 7.5) supplemented with 1 g/L bovine serum albumin, incubated with a 1:4000 dilution of anti-digoxigenin alkaline phosphatase F_{ab} fragments (Roche Applied Science, Indianapolis, Indiana, United States). Wing discs were then washed ten times (10-120 min per wash) in cold TBST, followed by an incubation in an alkaline phosphatase buffer (100 mM Tris-HCl pH 9.5, 100 mM NaCl, 5 mM MgCl₂, 0.01% Tween20), and finally stained with BM Purple (Roche Applied Science) for 4-8hr at room temperature. Stained tissues were then washed three times in PBST 2 mM ethylene diamine tetraacetic acid for 5 minutes each time incubated in PBS containing 60% glycerol for 1h. Wing discs were mounted onto slides in PBS containing 60% glycerol and

mRNA *in situ* hybridizations were photographed with a Nikon Coolpix P5100 digital camera (Nikon USA, Melville, New York, United States) mounted with a LNS- 30D/P51 adaptor (Zarf Enterprises, Spokane, Washington, United States) on a Leica S4E microscope (Leica Microsystems, Buffalo Grove, Illinois, United States). All the presented results were replicated in at least three individuals per morph at informative stages.

Immunofluorescence

To compare the localization of Optix protein in wild-type and *WntA* KO pupal wings we performed immunofluorescence using anti optix-antisera ([Figure 5](#)). Pupae were cold-anesthetized and dissected in PBS. Pupal forewings were incubated in fixative (PBS, 2 mM EGTA, 1.85% formaldehyde) for 30 min at room temperature while still attached to their cuticle. Similarly, and in order to maintain flat wing tissues, hindwings were kept attached to their pupal case and fixed for at least 5 min as such, then detached by dissection, and left for the remainder of the 30 min fixation as free-floating wings. Fixed wings were washed five times with PBST (PBS, 0.5% Triton X-100) and stored at 4°C for up to two months. Before beginning immunostaining, wings were cleaned from remnants of peri-podial membrane using fine forceps and then incubated in blocking buffer for 2 hr (PBS, 0.5% Triton X-100, 5% Normal Goat Serum; at room temperature), followed by an overnight incubation at 4°C with anti-optix polyclonal rat serum (dilution 1:3000). The following morning, wings were washed six times with PBST and then incubated for 2 hr at room temperature with an anti- rat IgG Alexa488 antibody (Cell Signaling Technology, Danvers, Massachusetts, USA; 1:2000 dilution). Tissues were then washed five times in PBST at room temperature for five minutes each time and incubated in glycerol (PBS, 60% glycerol, 2 mM ethylenediaminetetraacetic acid) for one hour. The wings were then mounted on slides and observed with an Olympus FV1000 confocal microscope.

QUANTIFICATION AND STATISTICAL ANALYSIS

Automated image analysis of clonal mutant butterflies

The clonal nature of CRISPR/Cas9 mosaic knockouts presents a challenging phenotypic analysis. Clones vary in size, and while some mutant clones will encompass the whole wing, many wings will contain one or a number of unconnected clones. To get a holistic sense of the full range of knockout phenotypes that are possible, we performed automated image analysis on mutants using the R package *patternize* [[40](#)]. For each pair of co-mimetic species (*H. cydno* & *H. sapho*, *H. pachinus* & *H. hewitsonii*, and *H. melpomene* & *H. erato*), a minimum of 5 Wild-Type and 5 *WntA* KO dorsal forewings were photographed and landmarked according to the scheme used by Van Belleghem et al. [[40](#)]. Appropriate RGB values were selected for the non-black pattern elements in each species, and images were registered into raster layers using the patLanRGB module. Raster layers for Wild-Types and *WntA* mutants were summed, and the difference between the two groups calculated and converted into heatmaps on a spectrum of -1 (white) to +1 (color), where +1 indicates pattern that is present in the mutants but absent in the wild-types, and -1 indicating pattern that is present in the wild-types but absent in the mutants.

Quantitative analysis of wing scale morphology and ultrastructure

In order to assess if *WntA* function is required for the correct development of wing scale ultrastructure, we performed Scanning Electron Microscopy (SEM) on wing scales from wild-type and mutant individuals. We first compared scale cell morphology between mutant and wild-type samples. For this, scales were removed from wings with a tungsten needle, immersed in clove oil, which has the same refractive index as the insect cuticle, and imaged on a Axioskop 2 plus (Carl Zeiss) microscope under a 40x objective with a Cannon 5DS camera. Scales were compared between wild-type and mutant butterflies for both proximal and middle wing regions on the forewing. Three biological replicates were used for *WntA* mutants and three wild-type replicates were used for controls. Five cover scales and five ground scales from each region from each individual were measured for length, width, and area in ImageJ ($n = 15$ per wing region per treatment). Length and Width were measured with the straight-line tool from furthest point to furthest point on the scale and area was measured independently by transforming files into black and white binary images and measuring area of the black (whole scale) with ImageJ. We only report results from cover scales because ground scales were found to not differ between wing regions, or scale coloration, between wild-type and mutant butterflies. The shape of scales was also assessed qualitatively, i.e., number of prongs on the ends of scales, to address if scale shape differed between wing colors.

We then compared the scale ultrastructure of wild-type and *WntA* mutants using SEM. Wings were cut into proximal and medium regions and were adhered to aluminum stubs using silver paste, followed by coating with 15 nm platinum and imaging on a JEOL JSM-6500F FE-SEM at 5 kV. Three scales for each wing region, for each individual were imaged at 10,000X ($n = 9$ per wing region per treatment). Measurements for lamella ridge distance and cross-rib distance were conducted in ImageJ, again using the straight-line tool and measured from furthest point to furthest point. For each individual scale image, a minimum of ten measurements from across the scale for both the lamella ridge and cross-rib distance were performed. These values were averaged to obtain an average cross-rib and lamella ridge distance per individual scale. Violin plots were generated in R Studio with the package ggplot2. To test for significant differences between treatments and scale colors, non-parametric statistical tests, Mann-Whitney U tests, were conducted in R studio using the package ggpubR.

DATA AND CODE AVAILABILITY

The software used for analysis of Illumina sequences obtained from *WntA* KO butterflies can be found in the following internet links:

FastQC v0.11.7

<http://www.bioinformatics.babraham.ac.uk/projects/fastqc/>

Trimmomatic v0.38

<http://www.usadellab.org/cms/?page=trimmomatic>

Most updated versions of COPE and CRISPResso are available at github

COPE v1.2.5

<https://github.com/dhlbh/COPE>

CRISPResso (Needle is within the program)

<https://github.com/lucapinello/CRISPResso>

The code used for the automated analysis of *WntA* KO wing patterns using *patternize* software is available at <https://github.com/Hanliconius>.

The software used for making violin plots and the corresponding statistical analysis of scale nanostructure measurements can be found in:

<https://CRAN.R-project.org/package=ggplot2>

<https://CRAN.R-project.org/package=ggpubr>